Error estimate of the Non-Intrusive Reduced Basis (NIRB) two-grid method with parabolic equations

October 31, 2022

Elise Grosjean [1], Yvon Maday [2] [3]

Abstract

Reduced Basis Methods (RBMs) are often proposed to approximate solutions of parametric problems. They are useful both to compute solutions for a large number of parameter values (e.g. for parameter fitting) and to approximate a solution for a new parameter value (e.g. real time approximation with a very high accuracy). They aim at reducing the computational costs of High Fidelity (HF) codes. They require well chosen solutions, called snapshots, preliminary computed (e.g. offline) with a HF classical method, involving, e.g. a fine mesh (finite element or finite volume) and generally require a profound modification of the HF code, in order for the online computation to be performed in short (or even real) time.
In this paper, we will focus on the Non-Intrusive Reduced Basis (NIRB) two-grid method. Its main advantage is its efficient way of using the HF code exclusively as a "black-box", unlike other so-called intrusive methods which require a modification of the code. This is very convenient when the HF code is a commercial one and has been purchased, as is often the case in the industry. The effectiveness of this method relies on its decomposition into two stages, one offline (classical in most RBMs as presented above) and one online. The offline part is time-consuming but it is executed only once. On the contrary, the specificity of the NIRB approach is to solve, during the online part, the parametric problem on a coarse mesh only, and then to improve its precision. It is thus much cheaper than a HF evaluation. This method has been initially developed in the context of elliptic equations with finite element and has been extended to finite volume.
In this paper, we generalize the NIRB two-grid method to parabolic equations. To the best of our knowledge, the two-grid method has not already been studied in the context of time-dependent problems. With a model problem, which is the heat equation, we recover optimal estimates in $L^\infty(0,T;H^1(\Omega))$, and present numerical results.

1 Introduction

Let Ω be a bounded domain in $\mathbb{R}^d$, with $d \leq 3$ with smooth enough boundary $\partial\Omega$, and let us consider a parametric problem $\mathcal{P}$ on Ω. Non-Intrusive Reduced Basis (NIRB) methods are an alternative to classical Reduced Basis Methods (RBMs) to approximate the solutions of such problems where the parameter is denoted as μ, in a given set $\mathcal{G}$ [8, 9] (see also different NIRB methods [5, 1] from the two-grid method). They may be more pratical to implement than intrusive RBMs from an engineering point of view and they only require the execution of the High-Fidelity (HF) code only as a "black-box" solver. Like most RBMs, the NIRB methods rely on the assumption that the manifold of all solutions $\mathcal{S} = \{u(\mu), \mu \in \mathcal{G}\}$ has a small Kolmogorov width [18] (in what follows, $u_h(\mu)$ will refer to the HF solution for the parameter μ).

1.1 Reminders on the NIRB two-grid method for stationnary problems

The two-grid method, in the context of a HF solver of finite element or finite volume type, involves two partitioned meshes (or "grid"), one fine mesh $\mathcal{M}_h$ and one coarse $\mathcal{M}_H$, where the respective sizes h and H of the

[1] Felix-Klein-Institut für Mathematik, Kaiserslautern TU, 67657, Deutschland
[2] Sorbonne Université and Université de Paris Cité, CNRS, Laboratoire Jacques-Louis Lions (LJLL), F-75005 Paris, France
[3] Institut Universitaire de France

meshes are such that $h << H$. The size h (respectively H) is defined as

$$h = \max_{K \in \mathcal{M}_h} h_K \text{ (respectively } H = \max_{K \in \mathcal{M}_H} H_K), \tag{1}$$

where the diameter h_K (or H_K) of any element K in a mesh is equal to $\sup_{x,y \in K} |x - y|, K \in M_h$ (or $\in M_H$).

The fine mesh is used for the construction of the Reduced Basis (RB). The reduced space denoted $X_h^N := Span\{u_h(\mu_i) \; | i = 1, \dots N\}$ is generated with N snapshots. Then, the solution for a new parameter is roughly and rapidly approximated with a coarse mesh. The latter and the offline-online decomposition of the algorithm are the key ingredients to the reduction of the complexity. Thus, we carry out the following decomposition:

- First, the RB functions which belong to the reduced space denoted X_h^N are prepared in an "offline" stage with the fine mesh through a greedy procedure [4, 22] (an alternative is to use a Proper Orthogonal Decomposition (POD) [2, 16]). The greedy procedure is a way to compute the modes by choosing iteratively some suitable parameters $\mu_1, \dots, \mu_N \in \mathcal{G}$ and computes the approximate solutions $u_h(\mu_1), \dots, u_h(\mu_N)$. This part is costly in time, but only executed once, as for other RBMs. At the end of this stage, we obtain N L^2-orthonormalized basis functions, denoted $(\Phi_i^h)_{i=1,\dots,N}$, after processing a Gram-Schmidt orthonormalization algorithm. In order to enhance the results (as we will detail in section 4), we may further perform the following eigenvalue problem:

$$\begin{cases} \text{Find } \Phi^h \in X_h^N, \text{ and } \lambda \in \mathbb{R} \text{ such that:} \\ \forall v \in X_h^N, \int_\Omega \nabla \Phi^h \cdot \nabla v \; d\mathbf{x} = \lambda \int_\Omega \Phi^h \cdot v \; d\mathbf{x}, \end{cases} \tag{2}$$

  and we get an increasing sequence of eigenvalues λ_i, and orthogonal eigenfunctions $(\Phi_i^h)_{i=1,\cdots,N}$, orthonormalized in $L^2(\Omega)$ and thus orthogonal in $H^1(\Omega)$, and define a new basis of the space X_h^N.

- Then, for a new parameter $\mu \in \mathcal{G}$ for which we are interested in estimating the solution, a coarse approximation of the solution, denoted $u_H(\mu)$, is first computed "online". This coarse approximation is, of course, not of sufficient precision but it is calculated much more rapidly compared to the HF one. The NIRB post-processing then notably improves the precision by projecting $u_H(\mu)$ on the RB, within a very short runtime [8, 6, 12, 9]. The classical NIRB approximation is given by

$$u_{Hh}^N(\mu) := \sum_{i=1}^N (u_H(\mu), \Phi_i^h) \; \Phi_i^h.$$

  We remark that, for a new parameter $\mu_k \in \mathcal{G}$, $u_{Hh}^N(\mu_k)$ differs from $u_h(\mu_k)$ (as numerically shown in section 5). As proposed in [7], in order to cover this and improve the accuracy, we introduce a rectification matrix, denoted $\mathbf{R}$. In addition to the fine snapshots, the construction of this matrix employs coarse snapshots which are generated with the same parameters as for the fine snapshots (during the offline part). Then, we compute the vectors

$$\mathbf{R}_i = (\mathbf{A}^T\mathbf{A} + \delta \mathbf{I}_N)^{-1}\mathbf{A}^T\mathbf{B}_i, \; i = 1, \cdots, N, \tag{3}$$

  where

$$\forall i = 1, \cdots, N, \text{ and } \forall \mu_k \in \mathcal{G},$$

$$A_{k,i} = \int_\Omega \mathbf{u}_H(\mu_k) \cdot \Phi_i^h \; d\mathbf{x}, \tag{4}$$

$$B_{k,i} = \int_\Omega \mathbf{u}_h(\mu_k) \cdot \Phi_i^h \; d\mathbf{x}, \tag{5}$$

  where $\mathbf{I}_N$ refers to the identity matrix and δ is a regularization term [8]. The post-treatment applied to NIRB approximation reads

$$Ru_{Hh}^N(\mu) := \sum_{i,j=1}^N R_{ij} \; (u_H(\mu), \Phi_j^h) \; \Phi_i^h,$$

  where $(\cdot, \cdot)$ denotes the L^2-inner product. Note that, when the relaxation parameter $\delta = 0$ the rectification process allows to retrieve the fine coefficients (given in (5)) from the coarse ones (given in (4)) for the parameters $\mu = \mu_k$, $k = 1, \dots, N$. In other words, with $\delta = 0$, we have

$$Ru_{Hh}^N(\mu_k) = u_h(\mu_k), \quad k = 1, \dots, N.$$

1.2 Motivation and earlier works.

The two-grid method can be used for several types of PDEs and approximations and is easy to implement. Moreover, its non-intrusive nature makes it appealing for a wide range of problems. Yet, to the best of our knowledge, this method has not already been studied nor implemented in the context of time-dependent problems [6, 8, 9, 23].
The two-grid method has been developed and analyzed in the context of $\mathbb{P}_1$ FEM (with Céa's and Aubin-Nitsche's lemmas) in [7] for second order elliptic equations. The energy-error estimate then is given by

$$\left\| u(\mu) - u_{Hh}^N(\mu) \right\|_{H^1(\Omega)} \leq \varepsilon(N) + C_1 h + C_2(N) H^2, \tag{6}$$

where C_1 and C_2 are constants independent of h and H, C_2 depends on N only. The term $\varepsilon(N)$ depends on a proper choice of the RB space as a surrogate for the best approximation space associated to the Kolmogorov N-width. It decreases when N increases and it is linked to the error between the fine solution and its projection on X_h^N, given by

$$\left\| u_h(\mu) - \sum_{i=1}^{N} (u_h(\mu), \Phi_i^h)\ \Phi_i^h \right\|_{H^1(\Omega)}. \tag{7}$$

The second term in (6), $C_1\ h$, is a contribution obtained through Céa's lemma for the RB elements and the second one, $C_2(N)\ H^2$, through Aubin-Nitsche's lemma for the coarse grid approximation of $u(\mu)$. The constant C_2 increases with N and thus, a trade-off needs to be done between increasing N to obtain a more accurate manifold, and keeping a constant C_2 as low as possible.
This two-grid method has also been generalized and analyzed in the context of finite volume schemes [12] where a surrogate to Aubin-Nitsche's is used.

1.3 Outline of the paper.

This article is about extending NIRB to time-dependent problems and performing its numerical analysis, in the setting of parabolic equations.
We will first theoretically prove that we can recover optimal estimates in $L^\infty(0,T;H^1(\Omega))$, and then present numerical results 5. Our main result is given by the theorem 4.1 on the numerical analysis of convergence of the approach.
The rest of this paper is organized as follows. In section 2 we describe the mathematical context. In section 3 we present the two-grids method in the context of parabolic equations. Section 4 is devoted to the proof of theorem 4.1. In the last section 5, the implementation is discussed and we illustrate the theoretical results with numerical results on the NIRB method with and without rectification.
In the next sections, C will denote various positive constants independent of the size of the meshes h and H and of the parameter μ, and $C(\mu)$ will denote constants independent of the sizes of the meshes h and H but dependent of μ.

2 Mathematical Background

2.1 The continuous problem

We will consider the following heat equation on the domain Ω with homogeneous Dirichlet conditions, which takes the form

$$\begin{aligned} u_t - \mu\Delta u &= f, \quad \text{in } \Omega\times]0,T], \\ u(\mathbf{x},0) &= u_0(\mathbf{x}), \quad \text{in } \Omega, \\ u(\mathbf{x},t) &= 0, \quad \text{on } \partial\Omega\times]0,T], \end{aligned} \tag{8}$$

where $f \in L^2(\Omega\times[0,T])$, for any $t > 0$, $u(\cdot,t) \in H_0^1(\Omega)$, $u_t(\cdot,t) \in L^2(\Omega)$ stands for the derivative of u with respect to time, $u_0 \in H_0^1(\Omega)$ and $0 < \mu \in \mathcal{G}$ is the parameter.

We use the conventional notations for space-time dependent Sobolev spaces

$$L^p(0,T;V) := \{u(\mathbf{x},t) \mid \|u\|_{L^p(0,T;V)} := \Big(\int_0^T \big\|u(\cdot,t)\big\|_V^p \ dt \Big)^{1/p} < \infty\}, \ 1 \leq p < \infty,$$
$$L^\infty(0,T;V) := \{u(\mathbf{x},t) \mid \|u\|_{L^\infty(0,T;V)} := ess \sup_{0\leq t\leq T} \big\|u(\cdot,t)\big\|_V < \infty\},$$

where V is a real Banach space with norm $\|\cdot\|_V$. The variational form of (8) is given by:

$$\begin{cases} \text{Find } u \in L^2(0,T;H_0^1(\Omega)) \text{ with } u_t \in L^2(0,T;H^{-1}(\Omega)) \text{ such that} \\ (u_t,v) + a(u,v;\mu) = (f,v), \ \forall v \in H_0^1(\Omega) \text{ and } t \in (0,T), \\ u(\cdot,0) = u_0, \text{ in } \Omega, \end{cases} \tag{9}$$

where a is given by

$$a(w,v;\mu) = \int_\Omega \mu \nabla w(\mathbf{x}) \cdot \nabla v(\mathbf{x}) \ d\mathbf{x}, \quad \forall w,v \in H_0^1(\Omega). \tag{10}$$

We remind that (9) is well posed (see [10] for the existence and the uniqueness of solutions to problem (9)) and we refer to the notations of [10].

Remark 2.1. *(On the stability). We intend to state estimates for the NIRB approximation for all time snapshots n, that is related to maximum-norm in time with the either L^2 norm or H^1 norm in space, ie in $L^\infty(0,T;L^2(\Omega))$ and $L^\infty(0,T;H^1(\Omega))$, which is stronger than with the usual stability study of the parabolic equation* (8)*. Let us remind the classical (or less standard) stability results. We derive from* (9) *by using $v = u$*

$$(u_t,u) + \mu\|\nabla u\|^2 = |(f,u)|. \tag{11}$$

From the Young and Poincaré inequalities, there exists $C > 0$ such that

$$|(f,u)| \leq (\frac{1}{2\mu}\|f\|^2) + \frac{\mu}{2}\|\nabla u\|^2.$$

and since

$$(u_t,u) = \frac{1}{2}\frac{d}{dt}\|u\|^2,$$

(11) *yields*

$$\frac{d}{dt}\|u\|^2 + \mu\|\nabla u\|^2 \leq \frac{1}{\mu}\|f\|^2,$$

and integrating over $(0,t)$ for all $t \leq T$, we end up with

$$\big\|u(t)\big\|^2 + \mu \int_0^t \big\|\nabla u(s)\big\|^2 \ ds \leq C(\|u_0\|^2 + \frac{1}{\mu}\int_0^t \big\|f(s)\big\|^2 \ ds),$$

which gives

$$\|u\|^2_{L^\infty(0,T;L^2(\Omega))} + \mu\|u\|^2_{L^2(0,T;H_0^1(\Omega))} \leq C(\|u_0\|^2_{L^2(\Omega)} + \frac{1}{\mu}\|f\|^2_{L^2(0,T;L^2(\Omega))}).$$

That establishes the first stability result.
For the L^∞ stability in time and H^1 in space, we proceed the same with $v = u_t$ in (9)*. Integrating over $(0,t)$ for all $t \leq T$, it yields*

$$\int_0^t \big\|u_t(s)\big\|^2 \ ds + \mu \int_0^t \frac{d}{dt}\big\|\nabla u(s)\big\|^2 \ ds \leq \int_0^t \big\|f(s)\big\|^2 \ ds,$$

which gives

$$\int_0^t \big\|u_t(s)\big\|^2 \ ds + \mu\big\|\nabla u(t)\big\|^2 \leq \mu \ \|\nabla u_0\|^2 + \int_0^t \big\|f(s)\big\|^2 \ ds,$$

and we obtain

$$\|u\|^2_{L^\infty(0,T;H_0^1(\Omega))} \leq \|\nabla u_0\|^2_{L^2(\Omega)} + \frac{1}{\mu}\big\|f(s)\big\|^2_{L^2(0,T;L^2(\Omega))}.$$

2.2 The various discretizations

Like in the previous work on the NIRB FEM applied to elliptic equations [7], we consider one fine spatial grid for computing "offline" the snapshots associated with few values of the parameter and one coarse grid for the coarse solution, with sizes respectively denoted as h and H (with $h << H$) (1). These grids are used for the spacial discretizations of the weak formulation of problem (8). We employed $\mathbb{P}_1$ finite elements for the discretization in space, thus let V_h and V_H consists of continuous piecewise linear finite element functions (respectively on the fine and coarse mesh) which vanish on the boundary $\partial\Omega$. We consider the projection operator P_h^1 on V_h (P_H^1 on V_H is defined similarly) which is given by

$$(\nabla P_h^1 u, \nabla v) = (\nabla u, \nabla v), \quad \forall v \in V_h, \tag{12}$$

Now, a time stepping method of finite difference type is used to get a fully discrete approximation of the solution of (8). We consider two different time grids:

- One time grid, denoted F, is employed for the fine solution (for the snapshots construction). To avoid making notations more cumbersome, we will consider a uniform time step Δt_F. The time levels can be written $t^n = n\ \Delta t_F$, where $n \in \mathbb{N}^*$.
- Another time grid, denoted G, is used for the coarse solution. By analogy with the fine grid, we consider a uniform grid with time step Δt_G. Now, the time levels are written $\widetilde{t}^m = m\ \Delta t_G$, where $m \in \mathbb{N}^*$.

Now, the NIRB algorithm allows us to recover the optimal estimate in space, as in the previous analysis with elliptic equations. Yet, there is no such argument as the Aubin-Nitsche's one for time stepping method, hence we need to consider time discretizations that provide the same precision with different time steps hence we consider a higher order time scheme for the coarse solution. Here, we will use an Euler scheme for the fine solution and Crank-Nicolson scheme for the coarse one.
Thus, we deal with two kind of notations:

- $u_h(\mathbf{x}, t)$ and $u_H(\mathbf{x}, t)$ that respectively denote the fine and coarse solutions of the spatially semi-discrete solution, at time $t \geq 0$.
- $u_h^n(\mathbf{x})$ and $u_H^m(\mathbf{x})$ that respectively denote the fine and coarse full-discretized solutions at time $t^n = n \times \Delta t_F$ and $\widetilde{t}^m = m \times \Delta t_G$.

Remark 2.2. *To simplify the notations, we consider that both time simulations end at time T here,*

$$T \ = \ N_T \Delta t_F \ = \ M_T \Delta t_G.$$

The semi-discrete form of the variational problem (9) writes for the fine mesh (similarly for the coarse mesh):

$$\begin{cases} \text{Find } u_h(t) = u_h(\cdot, t) \in V_h \text{ for } t \geq 0 \text{ such that} \\ (\partial_t u_h, v_h) + a(u_h, v_h; \mu) = (f(t), v_h),\ \forall v_h \in V_h \text{ and } n \geq 1, \\ u_h(\cdot, 0) \ = \ u_h^0 \ = \ P_h^1(u^0), \end{cases} \tag{13}$$

The full discrete form of the variational problem (9) for the fine mesh with implicit Euler scheme writes:

$$\begin{cases} \text{Find } u_h^n \in V_h \text{ for } n \geq 0 \text{ such that} \\ (\overline{\partial} u_h^n, v_h) + a(u_h^n, v_h; \mu) = (f(t^n), v_h),\ \forall v_h \in V_h \text{ and } n \geq 1, \\ u_h(\cdot, 0) \ = \ u_h^0, \end{cases} \tag{14}$$

where the time derivative in the variational form of the problem (13) has been replaced by a backward difference quotient, $\overline{\partial} u_h^n = \frac{u_h^n - u_h^{n-1}}{\Delta t_F}$, and with Crank-Nicolson scheme, and $\overline{\partial} u_H^m = \frac{u_H^m - u_H^{m-1}}{\Delta t_G}$, it becomes, for the coarse mesh:

$$\begin{cases} \text{Find } u_H^m \in V_H \text{ for } m \geq 0, \text{ such that} \\ (\overline{\partial} u_H^m, v_H) + a(\frac{u_H^m + u_H^{m-1}}{2}, v_H; \mu) = (f(\widetilde{t}^{m-\frac{1}{2}}), v_H),\ \forall v_H \in V_H \text{ and } m \geq 1, \\ u_H(\cdot, 0) \ = \ u_H^0, \end{cases} \tag{15}$$

where $\widetilde{t}^{m-\frac{1}{2}} = \frac{\widetilde{t}^m + \widetilde{t}^{m-1}}{2}$.

Let us remind a few results from [24], on the FEM classical estimates and on both finite difference schemes employed. In the following theorems, we require that the solution u of the continuous problem has the regularity implicitly assumed by the presence of the norms on the right. It is well known that with a FEM semi-discretization in space, the following estimates hold:

Theorem 2.3 (Theorem 1.2 [24]). *Let Ω be a convex polyhedron. Let $u \in W^{1,1}(0,T;H^2(\Omega))$ be the solution of* (8) *with $u_0 \in H^2(\Omega)$ and u_h be the semidiscretized variational form* (13)*. Then*

$$\text{for } t \geq 0, \quad \left\|u(t) - u_h(t)\right\|_{L^2(\Omega)} \leq C(\mu)h^2\left[\|u_0\|_{H^2(\Omega)} + \int_0^t \|u_t\|_{H^2(\Omega)}\ ds\right], \tag{16}$$

Once fully discretized on a fine mesh with the backward Euler Galerkin method, the estimate (16) is replaced by the following estimate.

Theorem 2.4 (Theorem 1.5 [24]). *Let Ω be a convex polyhedron and. With u_h^n and u be the solutions of* (14) *and* (8)*, respectively. If $\left\|u_h^0 - u_0\right\|_{L^2(\Omega)} \leq Ch^2\|u_0\|_{H^2(\Omega)}$, we have*

$$\forall n \geq 0 \quad ,\left\|u(t^n) - u_h^n\right\|_{L^2(\Omega)} \leq C(\mu)h^2\left[\|u_0\|_{H^2(\Omega)} + \int_0^{t^n} \|u_t\|_{H^2(\Omega)}\ ds\right] + C(\mu)\ \Delta t_F \int_0^{t^n} \|u_{tt}\|_{L^2(\Omega)}\ ds, \tag{17}$$

Theorem 2.5 (Theorem 1.4 [24]). *Let Ω be a convex polyhedron. Let $u \in H^1(0,T;H^2(\Omega)) \cap L^2(0,T;H^2(\Omega))$ be the solution of* (8) *with $u_0 \in H^2(\Omega)$ and u_h be the semidiscretized variational form* (13)*, we have*

$$\text{for } t \geq 0, \quad \left\|\nabla u(t) - \nabla u_h(t)\right\|_{L^2(\Omega)} \leq C(\mu)h\left[\|u_0\|_{H^2(\Omega)} + \left\|u(t)\right\|_{H^2(\Omega)} + (\int_0^t \|u_t\|_{H^1(\Omega)}^2\ ds)^{1/2}\right]. \tag{18}$$

The estimate (18) with the full discretization leads to the following theorem.

Theorem 2.6. *Let Ω be a convex polyhedron. Let $u \in H^1(0,T;H^2(\Omega)) \cap H^2(0,T;L^2(\Omega))$ be the solution of* (8) *with $u_0 \in H^2(\Omega)$ and u_h be the semidiscretized variational form* (13)*, we have*

$$\begin{aligned}\forall n \geq 0, \quad \left\|\nabla u_h^n - \nabla u(t^n)\right\|_{L^2(\Omega)} \leq & C(\mu)h\left[\|u_0\|_{H^2(\Omega)} + (\int_0^{t^n} \|u_t\|_{H^2(\Omega)}^2\ ds)^{1/2}\right] \\ & + C(\mu)\ \Delta t_F(\int_0^{t^n} \|\nabla u_{tt}\|_{L^2(\Omega)}^2\ ds)^{1/2}.\end{aligned} \tag{19}$$

Proof. This may be proven by following the same lines as in the proof on the L^2 estimate (Theorem 1.5 [24]), as it is highlighted in [24]. We first decompose the error with two components θ and ρ such that

$$\begin{aligned}\forall n \geq 1,\ e^n &:= \sqrt{\mu}(\nabla u_h^n - \nabla u(t^n)) = \sqrt{\mu}((\nabla u_h^n - \nabla P_h^1 u(t^n)) + (\nabla P_h^1 u(t^n) - \nabla u(t^n))) \\ &= \sqrt{\mu}(\nabla\theta^n + \nabla\rho^n).\end{aligned} \tag{20}$$

- For the estimate on ρ^n, a classical FEM estimate [24, 3] is

$$\left\|P_h^1 v - v\right\|_{L^2(\Omega)} + h\left\|\nabla(P_h^1 v - v)\right\|_{L^2(\Omega)} \leq Ch^2\|v\|_{H^2(\Omega)}, \quad v \in H^2 \cap H_0^1,$$

  which leads to

$$\left\|\nabla\rho^n\right\|_{L^2(\Omega)} \leq Ch\left\|u(t^n)\right\|_{H^2(\Omega)}, \ \forall n \geq 0,$$

  and it leads to ,

$$\left\|\nabla\rho^n\right\|_{L^2(\Omega)} \leq Ch\left[\|u_0\|_{H^2(\Omega)} + \int_0^{t^n} \|u_t\|_{H^2(\Omega)}\ ds\right]. \tag{21}$$

- For the estimate on θ, let us consider $v \in V_h$. Since the operators P_h^1 and $\overline{\partial}$ commute, we write

$$(\overline{\partial}\theta^n, v) + \mu(\nabla\theta^n, \nabla v) = (\overline{\partial}u_h^n, v) - (P_h^1\overline{\partial}u(t^n), v) + \mu(\nabla u_h^n, \nabla v) - \mu(\nabla P_h^1 u(t^n), \nabla v).$$

From (9) and (14), it implies

$$\begin{aligned}(\overline{\partial}\theta^n, v) + \mu(\nabla\theta^n, \nabla v) &= (f, v) - (P_h^1\overline{\partial}u(t^n), v) - \mu(\nabla P_h^1 u(t^n), \nabla v),\\ &= (f, v) - (P_h^1\overline{\partial}u(t^n), v) - \mu(\nabla u(t^n), \nabla v), \text{ by definition of } P_h^1,\\ &= (u_t(t^n), v) - (P_h^1\overline{\partial}u(t^n), v).\end{aligned}$$

Then, with a triangle inequality, it yields

$$\begin{aligned}(\overline{\partial}\theta^n, v) + \mu(\nabla\theta^n, \nabla v) &= -((P_h^1 - I)\overline{\partial}u(t^n), v) - ((\overline{\partial}u(t^n) - u_t(t^n)), v)\\ &:= -(w_1^n + w_2^n, v) = -(w^n, v).\end{aligned} \tag{22}$$

Instead of replacing v by θ^n as in the L^2 estimate, here we replace v by $\overline{\partial}\theta^n$, thus the equation (22) takes the form

$$(\overline{\partial}\theta^n, \overline{\partial}\theta^n) + \mu(\nabla\theta^n, \overline{\partial}\nabla\theta^n) = -(w^n, \overline{\partial}\theta^n).$$

Therefore, by definition of $\overline{\partial}$ for the Backward Euler discretization,

$$\underbrace{(\overline{\partial}\theta^n, \overline{\partial}\theta^n) + \mu\frac{\|\nabla\theta^n\|^2_{L^2(\Omega)}}{\Delta t_F} - \mu\frac{(\nabla\theta^n, \nabla\theta^{n-1})}{\Delta t_F}}_{T_a} = -(w^n, \overline{\partial}\theta^n).$$

With Young's inequality,

$$(\nabla\theta^n, \nabla\theta^{n-1}) \leq \frac{1}{2}\|\nabla\theta^n\|^2_{L^2(\Omega)} + \frac{1}{2}\left\|\nabla\theta^{n-1}\right\|^2_{L^2(\Omega)}.$$

Thus,

$$\left\|\overline{\partial}\theta^n\right\|^2_{L^2(\Omega)} + \mu\frac{\|\nabla\theta^n\|^2_{L^2(\Omega)}}{2\Delta t_F} - \mu\frac{\left\|\nabla\theta^{n-1}\right\|^2_{L^2(\Omega)}}{2\Delta t_F} \leq T_a \leq \frac{1}{2}\|w^n\|^2_{L^2(\Omega)} + \frac{1}{2}\left\|\overline{\partial}\theta^n\right\|^2_{L^2(\Omega)},$$

and it results in

$$\left\|\overline{\partial}\theta^n\right\|^2_{L^2(\Omega)} + \mu\frac{\|\nabla\theta^n\|^2_{L^2(\Omega)}}{\Delta t_F} \leq \mu\frac{\left\|\nabla\theta^{n-1}\right\|^2_{L^2(\Omega)}}{\Delta t_F} + \|w^n\|^2_{L^2(\Omega)}.$$

Since $\left\|\overline{\partial}\theta^n\right\|^2_{L^2(\Omega)} \geq 0$, it follows that

$$\forall n \geq 1,\ \|\nabla\theta^n\|^2_{L^2(\Omega)} \leq \left\|\nabla\theta^{n-1}\right\|^2_{L^2(\Omega)} + \frac{\Delta t_F}{\mu}\|w^n\|^2_{L^2(\Omega)},$$

and we recursively obtain

$$\forall n \geq 1,\ \|\nabla\theta^n\|^2_{L^2(\Omega)} \leq \left\|\nabla\theta^0\right\|^2_{L^2(\Omega)} + \frac{\Delta t_F}{\mu}\sum_{j=1}^{n}\left\|w^j\right\|^2_{L^2(\Omega)}.$$

By definition of θ (and P_h^1),

$$\begin{aligned}\left\|\nabla\theta^0\right\|_{L^2(\Omega)} &= \left\|\nabla u_h^0 - \nabla P_h^1 u(t^0)\right\|_{L^2(\Omega)} \leq \left\|\nabla u_h^0 - \nabla u(t^0)\right\|_{L^2(\Omega)} + \left\|\nabla u(t^0) - \nabla P_h^1 u(t^0)\right\|_{L^2(\Omega)}\\ &\leq \left\|\nabla u_h^0 - \nabla u(t^0)\right\|_{L^2(\Omega)} + Ch\left\|u(t^0)\right\|_{H^2(\Omega)}.\end{aligned}$$

It remains to estimate the L^2 norm of the w^j, defined by (22).

–

$$
\begin{aligned}
w_1^j &= (P_h^1 - I)\overline{\partial} u(t^j) \\
&= \frac{1}{\Delta t_F}(P_h^1 - I)\int_{t^{j-1}}^{t^j} u_t \, ds, \\
&= \frac{1}{\Delta t_F}\int_{t^{j-1}}^{t^j} (P_h^1 - I) u_t \, ds, \text{ since } P_h^1 \text{ and the time integral commute.}
\end{aligned}
$$

Thus, from Hölder's inequality,

$$
\begin{aligned}
\frac{\Delta t_F}{\mu}\sum_{j=1}^{n}\left\|w_1^j\right\|_{L^2(\Omega)}^2 &\leq \frac{\Delta t_F}{\mu}\sum_{j=1}^{n}\int_\Omega [\frac{1}{\Delta t_F^2}\int_{t^{j-1}}^{t^j}((P_h^1 - I)u_t)^2 \, ds \Delta t_F] \\
&\leq \frac{1}{\mu}\sum_{j=1}^{n}\int_{t^{j-1}}^{t^j}\left\|(P_h^1 - I)u_t\right\|_{L^2(\Omega)}^2 \, ds, \\
&\leq \frac{C}{\mu}h^4\sum_{j=1}^{n}\int_{t^{j-1}}^{t^j}\|u_t\|_{H^2(\Omega)}^2, \text{ by the definition of }, P_h^1 \\
&\leq \frac{C}{\mu}h^4\int_0^{t^n}\|u_t\|_{H^2(\Omega)}^2 \, ds. \qquad (23)
\end{aligned}
$$

– To estimate the L^2 norm of the w_2, we write

$$
\begin{aligned}
w_2^j &= \frac{1}{\Delta t_F}(u(t^j) - u(t^{j-1})) - u_t(t^j), \\
&= -\frac{1}{\Delta t_F}\int_{t^{j-1}}^{t^j}(s - t^{j-1})u_{tt}(s) \, ds,
\end{aligned}
$$

such that we end up with

$$
\frac{\Delta t_F}{\mu}\sum_{j=1}^{n}\left\|w_2^j\right\|_{L^2(\Omega)}^2 \leq \frac{1}{\mu}\sum_{j=1}^{n}\left\|\int_{t^{j-1}}^{t^j}(s - t^{j-1})u_{tt}(s) \, ds\right\|_{L^2(\Omega)}^2 \leq \frac{\Delta t_F^2}{\mu}\int_0^{t^n}\|u_{tt}\|_{L^2(\Omega)}^2 \, ds.
$$

Combining the estimates on ρ and θ concludes the proof.

□

Finally, in the same manner, we can recover the estimate in H^2 and Δt_G^2 with the Crank-Nicolson scheme in the L^2 norm

Theorem 2.7 (Theorem 1.6 [24]). *Let u_H^m be the solution given by* (15)*, associated to Crank-Nicolson discretization with the coarse grids, and u be the solution of* (8) *belonging to $H^2(0,T;H^2(\Omega)) \cap H^3(0,T;L^2(\Omega))$ such that $u_0 \in H^2(\Omega)$. Let $\left\|u_0^H - u_0\right\|_{L^2(\Omega)} \leq CH^2\|u_0\|_{H^2(\Omega)}$, then*

$$
\begin{aligned}
\forall m \geq 0, \quad \left\|u(\widetilde{t}^m) - u_H^m\right\|_{L^2(\Omega)} &\leq C(\mu)H^2\left[\|u_0\|_{H^2(\Omega)} + \int_0^{\widetilde{t}^m}\|u_t\|_{H^2(\Omega)} \, ds\right] \\
&+ C(\mu)\Delta t_G^2[(\int_0^{\widetilde{t}^m}\|u_{ttt} \, ds\|_{L^2(\Omega)}^2)^{1/2} + (\int_0^{\widetilde{t}^m}\|\Delta u_{tt}\|_{L^2(\Omega)}^2 \, ds)^{1/2}]. \qquad (24)
\end{aligned}
$$

Now, let $\widetilde{u_H}^n$ be the quadratic interpolation in time of the coarse solution at time $t^n \in I_m = [\widetilde{t}^{m-1}, \widetilde{t}^m]$ defined on $[\widetilde{t}^{m-2}, \widetilde{t}^m]$ from the values u_H^{m-2}, u_H^{m-1}, and u_H^m, for all $m = 2, \ldots, M_T$. Thus, we define the parabola on $[\widetilde{t}^{m-2}, \widetilde{t}^m]$ with the values $u_H^{m-2}, u_H^{m-1}, u_H^m$:

For $m \geq 2$, $\forall n \in I_m = [\widetilde{t}^{m-1}, \widetilde{t}^{m}]$,

$$\widetilde{u_H}^n(\mu) = \frac{u_H^{m-2}(\mu)}{(\widetilde{t}^m - \widetilde{t}^{m-2})(\widetilde{t}^{m-2} - \widetilde{t}^{m-1})}\Big[-(t^n)^2 + (\widetilde{t}^{m-1} + \widetilde{t}^m)t^n - t^{m-1}t^m\Big]$$
$$+\frac{u_H^{m-1}(\mu)}{(\widetilde{t}^{m-2} - \widetilde{t}^{m-1})(\widetilde{t}^{m-1} - \widetilde{t}^{m})}\Big[-(t^n)^2 + (\widetilde{t}^{m} + \widetilde{t}^{m-2})t^n - t^{m}t^{m-2}\Big]$$
$$+\frac{u_H^{m}(\mu)}{(\widetilde{t}^{m-1} - \widetilde{t}^{m})(\widetilde{t}^{m} - \widetilde{t}^{m-2})}\Big[-(t^n)^2 + (\widetilde{t}^{m-2} + \widetilde{t}^{m-1})t^n - t^{m-2}t^{m-1}\Big]. \quad (25)$$

For $t^n \in I_1 = [\widetilde{t}^0, \widetilde{t}^1]$, we use the parabola defined by the values u_H^0, u_H^1, u_H^2. Note that we choose this interpolation in order to keep an approximation of order 2 in time Δt_G (it works also with other quadratic interpolations). With this interpolated approximation, we have the following result.

Corollary 2.8 (of Theorem 2.7)**.** *Let $\widetilde{u_H}^n$ be the quadratic interpolation in time of the coarse solution, defined above, and u be the solution of* (8) *belonging to $H^2(0,T;H^2(\Omega)) \cap H^3(0,T;L^2(\Omega))$ such that $u_0 \in H^2(\Omega)$. Let $\left\|u_0^H - u_0\right\|_{L^2(\Omega)} \leq CH^2\|u_0\|_{H^2(\Omega)}$, then*

$$\forall n \geq 0, \quad \left\|u(\widetilde{t}^n) - \widetilde{u_H}^n\right\|_{L^2(\Omega)} \leq C(\mu)H^2\left[\|u_0\|_{H^2(\Omega)} + \int_0^{\widetilde{t}^m} \|u_t\|_{H^2(\Omega)}\, ds\right]$$
$$+ C(\mu)\Delta t_G^2[(\int_0^{\widetilde{t}^m} \|u_{ttt}\, ds\|^2_{L^2(\Omega)})^{1/2} + (\int_0^{\widetilde{t}^m} \|\Delta u_{tt}\|^2_{L^2(\Omega)}\, ds)^{1/2}]. \quad (26)$$

3 The Non-Intrusive Reduced Basis method (NIRB) in the context of parabolic equations

3.1 Main steps

This section details the main steps of the two-grids method algorithm in the context of parabolic equations and more precisely how to employ a POD-Greedy algorithm [14, 13, 17] in order to define the RB. Indeed, in the time-discrete formulation, a single solution associated with a parameter $\mu \in \mathcal{G}$ consists of a sequence of possibly several hundred snapshots over time (each snapshot being a HF finite element approximation in space at time t^n, $n = 1, \ldots, N_T$). Hence, during the greedy algorithm, each greedy step is combined with a temporal compression step performed by a POD. Let us detail the different steps of our offline-online decomposition. The first three points are performed in the offline part, and the others are done online.

1. From the parameters $(\mu_i)_{i\in\{1,\ldots Ntrain\}}$, we compute fine snapshots $\{\mathbf{u}_h^n(\mu_i)\}_{i\in\{1,\ldots N\}}$ with the HF solver (solving problem (14)). We define $\mathcal{G}_{train} = \underset{i\in\{1,\ldots Ntrain\}}{\cup} \mu_i$.

2. We generate the RB functions (time-independent) $(\Phi_i^h)_{i=1,\cdots,N}$ through a POD-Greedy algorithm from the above snapshots, as presented in algorithm 1 below (or a full Greedy algorithm 2).

Algorithm 1 POD-Greedy algorithm

Input: N_{max}, $\{\mathbf{u}_h^n(\mu_1), \cdots, \mathbf{u}_h^n(\mu_{N_{train}})$ with $\mu_i \in \mathcal{G}_{train},\ n = 0, \ldots, N_T.\}$
Output: Reduced basis $\{\Phi_1^h, \cdots, \Phi_N^h\}$

Choose $\mu_1 = \underset{\mu \in \mathcal{G}_{train}}{\arg\max} \left\| \mathbf{u}_h^n(\mu) \right\|_{l^\infty(0,\ldots,N;L^2(\Omega))}$,
Then produce a family of L^2-orthonormalized modes $\Phi_1, \cdots, \Phi_{N_1}$ through a POD ($\{\mathbf{u}_h^n(\mu_1),\ n = 0, \ldots, N_T.\}$) (obtained with a small tolerance).
Set $\mathcal{G}_1 = \mu_1$ and $X_h^1 = \text{span}\{\Phi_1, \cdots, \Phi_{N_1}\}$.
while $\sum_{k=1}^{N} N_k < N_{max}$ **do**
$\mu_k = \arg \max_{\mu \in \mathcal{G}_{train}} \frac{\left\| \mathbf{u}_h^n(\mu) - P^{k-1}(\mathbf{u}_h^n(\mu)) \right\|_{L^\infty(0,T;L^2)}}{\left\| \mathbf{u}_h^n(\mu) \right\|_{L^\infty(0,T;L^2)}}$, with P^{k-1} defined by
$P^{k-1}(\mathbf{u}_h^n(\mu)) = \sum_{i=1}^{k-1} (\mathbf{u}_h^n(\mu), \Phi_i^h)_{L^2}\ \Phi_i^h$.
$\Phi_{N_{k-1}+1}, \ldots, \Phi_{N_k} = POD(\{\mathbf{u}_h^n(\mu_k) - P^{k-1}(\mathbf{u}_h^n(\mu)),\ n = 0, \ldots, N_T)$
Set $\mathcal{G}_k = \mathcal{G}_{k-1} \cup \mu_k$ and $X_h^k = X_h^{k-1} \oplus \text{span}\{\Phi_{k-1}, \cdot, \Phi_{N_k}\}$.
end while

Remark 3.1. *In the following standard greedy algorithm, a tolerance treshold is used instead of a priori given number of basis functions.*

Algorithm 2 Greedy algorithm

Input: tol, $\{\mathbf{u}_h^n(\mu_1), \cdots, \mathbf{u}_h^n(\mu_{N_{train}})$ with $\mu_i \in \mathcal{G}_{train} \subset \mathcal{G},\ n = 0, \ldots, N_T.\}$
Output: Reduced basis $\{\Phi_1^h, \cdots, \Phi_N^h\}$

Choose $\mu_1, n_1 = \underset{\mu \in \mathcal{G}_{train},\ n \in \{0,\ldots,N_T}{\arg\max} \left\| \mathbf{u}_h^n(\mu) \right\|_{L^2(\Omega)}$,
Set $\Phi_1 = \frac{\mathbf{u}_h^{n_1}(\mu_1)}{\left\| \mathbf{u}_h^{n_1}(\mu_1) \right\|_{L^2}}$
Set $\mathcal{G}_1 = \mu_1, n_1$ and $X_h^1 = \text{span}\{\Phi_1\}$.
for $k = 2$ to N **do**:
$\mu_k, n_k = \arg \max_{\mu \in \mathcal{G}_{train},\ n = \{0,\ldots,N_T}} \left\| \mathbf{u}_h^n(\mu) - P^{k-1}(\mathbf{u}_h^n(\mu)) \right\|_{L^2}$, with P^{k-1} defined as in POD-Greedy algorithm.
Compute $\widetilde{\Phi_k} = \mathbf{u}_h^{n_k}(\mu_k) - \sum_{i=1}^{k-1} (\mathbf{u}_h^n(\mu_k), \Phi_i)_{L^2} \Phi_i$ and set $\Phi_k = \frac{\widetilde{\Phi_k}}{\left\| \widetilde{\Phi_k} \right\|_{L^2}}$
Set $\mathcal{G}_k = \mathcal{G}_{k-1} \cup \mu_k$ and $X_h^k = X_h^{k-1} \oplus \text{span}\{\Phi_k\}$
Stop when $\left\| \mathbf{u}_h^n(\mu) - P^{k-1}(\mathbf{u}_h^n(\mu)) \right\|_{L^2} \leq tol\ \forall \mu \in \mathcal{G}_{train},\ \forall n = 0, \ldots, N_T$.
end for

Remark 3.2. *The term*

$$\left\| \mathbf{u}_h^n(\mu) - P^{k-1}(\mathbf{u}_h^n(\mu)) \right\|_{L^2(\Omega)} \tag{27}$$

can be calculated either with a set of training snapshots or evaluated with an a-posteriori estimate. Since at each step k, all sets added in the basis are in the orthogonal complement of X_h^{k-1}, it yields an L^2 orthogonal basis without further processing. In practice, the algorithm is halted with a stopping criterion such as an error threshold or a maximum number of basis functions to generate.

Then, we solve the following eigenvalue problem:

$$\begin{cases} \text{Find } \Phi_h \in X_h^N, \text{ and } \lambda \in \mathbb{R} \text{ such that:} \\ \forall v \in X_h^N, \int_\Omega \nabla \Phi_h \cdot \nabla v \, d\mathbf{x} = \lambda \int_\Omega \Phi_h \cdot v \, d\mathbf{x}, \end{cases} \tag{28}$$

where $X_h^N = Span\{\Phi_1^h, \dots, \Phi_N^h\}$. We get an increasing sequence of eigenvalues λ_i, and orthogonal eigenfunctions $(\Phi_i^h)_{i=1,\cdots,N}$, which do not depend on time, orthonormalized in $L^2(\Omega)$ and orthogonalized in $H^1(\Omega)$. Note that with Gram-Schmidt procedure, we only obtain an L^2-orthonormalized RB.

3. For the rectification post-treatment, we generate the equivalent coarse snapshots and the rectification matrix with algorithm 3. The coarse snapshots, which have the same parameter as for the HF snapshots, are quadratically interpolated in time (25), and we apply the following algorithm.

Algorithm 3 algorithm for the offline rectification post-treatment

Input: $\{\mathbf{u}_h^n(\mu_1) \cdots \mathbf{u}_h^n(\mu_{N_{train}}),$ with $\mu_i \in \mathcal{G}_{train}, \ n = 0, \dots, N_T\}$ and with the same parameter $\{\mathbf{u}_H^m(\mu_1), \cdots, \mathbf{u}_H^m(\mu_{N_{train}}),$ with $\mu_i \in \mathcal{G}_{train} \subset \mathcal{G}, \ m = 0, \dots, M_T\}$
Output: Rectification matrix $R_{i,j}^n, \ n = 0, \dots, N_T$.

Realize the quadratic interpolation of the coarse snapshots in time, denoted $\widetilde{\mathbf{u}_H}^n, \ n = 0, \dots, N_T$ with (25).
for $n = 0, \dots, N_T$: **do**
Calculate the fine and coarse coefficients
$\forall i = 1, \cdots, N,$ and $\forall \mu_k \in \mathcal{G}_{train}, \ A_{k,i}^n = \int_\Omega \widetilde{\mathbf{u}_H}^n(\mu_k), \cdot, \Phi_i^h \, d\mathbf{x}$, and $B_{k,i}^n = \int_\Omega \mathbf{u}_h^n(\mu_k) \cdot \Phi_i^h \, d\mathbf{x}$,
For $i = 1, \cdots, N$, set $\mathbf{R}_i^n = (\mathbf{A^n}^T \mathbf{A^n} + \delta \mathbf{I}_N)^{-1} \mathbf{A^n}^T \mathbf{B^n}_i$.
end for

4. Now for the online part, we solve the problem (8) on the coarse mesh $\mathcal{T}_H$ for a new parameter $\mu \in \mathcal{G}$ at each time step $m = 0, \dots, M_T$.
5. We quadratically interpolate in time the coarse solution on the fine time grid with (25).
6. Then, we linearly interpolate $\widetilde{u_H}^n(\mu)$ on the fine mesh in order to compute the L^2-inner product with the basis functions. The approximation used in the two-grid method is

$$\text{For } n = 0, \dots, N_T, \ u_{Hh}^{N,n}(\mu) := \sum_{i=1}^N (\widetilde{u_H}^n(\mu), \Phi_i^h) \ \Phi_i^h, \tag{29}$$

and with the rectification post-treatment step [8, 12], it becomes

$$R^n[u_{Hh}^N(\mu)] := \sum_{i=1}^N R_{ij}^n \ (\widetilde{u_H}^n(\mu), \Phi_j^h) \ \Phi_i^h, \tag{30}$$

where R^n is the rectification matrix at time t^n (see algorithm 3).

In the subsequent section, we demonstrate the optimal error in $L^\infty(0, T; H^1(\Omega))$.

4 NIRB error estimate with parabolic equations

Main result Our main result is the following theorem.

Theorem 4.1. *(NIRB error estimate for parabolic equations.) Let us consider the problem 8 and its exact solution $u(\boldsymbol{x}, t; \mu)$, and the full discretized solution to the problem 14. Let $(\Phi_i^h)_{i=1,\dots,N}$ be the L^2-orthonormalized and H^1-orthogonalized RB generated with the POD-greedy algorithm 1 from the fine solutions of (14), on a fine mesh of size h, with $\mathbb{P}_1$ FE for the spatial discretization, and a Backward Euler scheme for the time discretization. For $m = 0, \dots, M_T$, let $u_H^m(\mu)$ be the coarse approximation of (14) for $\mu \in \mathcal{G}$, on a coarse mesh of size H, with a $\mathbb{P}_1$ FEM for the spatial discretization, and a*

Crank-Nicolson scheme for the time discretization.

Let us consider the NIRB approximation, defined by (**??**) *and derived from these solutions. Then, the following estimate holds*

$$\text{for } n = 0, \dots, N_T, \left\| u(t^n)(\mu) - u_{Hh}^{N,n}(\mu) \right\|_{H^1(\Omega)} \leq \varepsilon(N) + C_1(\mu)h + C_2(N)H^2 + C_3(\mu)\Delta t_F + C_4(N)\Delta t_G^2, \tag{31}$$

where C_1, C_2, C_3 and C_4 are constants independent of h and H, Δt_F and Δt_G. The term ε depends on the Kolmogorov N-width and measures the error given by (7)*. If H is such as $H^2 \sim h$, $\Delta t_G^2 \sim \Delta t_F$, and $\varepsilon(N)$ is small enough, with $C_2(N)$ and $C_4(N)$ not too large, it results in an error estimate in $\mathcal{O}(h + \Delta t_F)$.*

Theorem 4.1 proves that the NIRB two grids method can be applied to parabolic problems. We recover optimal error estimates in $L^\infty(0, T; H^1(\Omega))$. The NIRB two-grids method does not yield to optimal result in time, thus our choice of finite difference schemes is motivated by the fact that we want the coarse solution to be coarser in space as well as in time, compared to the fine solution.

Remark 4.2. *This theorem can be generalized to $\mathbb{P}_k$ FEM space, with $k > 1$.*

With the L^2 norm, we obtain the following theorem.

Theorem 4.3. *With the same assumptions as in the theorem 4.1, with the L^2 orthonormalized RB, the following estimate holds*

$$\text{for } n = 0, \dots, \frac{\Delta t_F}{T}, \left\| u(t^n)(\mu) - u_{Hh}^{N,n}(\mu) \right\|_{L^2(\Omega)} \leq \varepsilon'(N) + C_1'(H^2 + \Delta t_G^2) + C_2'(h^2 + \Delta t_F), \tag{32}$$

where C_1' and C_2' are constants independent of h, H and N, and ε' depends on the Kolmogorov N-width, and corresponds to the L^2 error between the fine solution and its projection on the reduced space.

We now go on with the proof of Theorem 4.1.

Proof. The NIRB approximation at time step $n = 0, \dots, N_T$, for a new parameter $\mu \in \mathcal{G}$ is defined by (**??**). Thus, the triangle inequality gives

$$\forall t = n \times \Delta t_F, \tag{33}$$

$$\begin{aligned} \left\| u(t)(\mu) - u_{Hh}^{N,n}(\mu) \right\|_{H^1(\Omega)} &\leq \left\| u(t)(\mu) - u_h^n(\mu) \right\|_{H^1(\Omega)} + \left\| u_h^n(\mu) - u_{hh}^{N,n}(\mu) \right\|_{H^1(\Omega)} + \left\| u_{hh}^{N,n}(\mu) - u_{Hh}^{N,n}(\mu) \right\|_{H^1(\Omega)} \\ &=: T_1 + T_2 + T_3, \end{aligned} \tag{34}$$

where $u_{hh}^{N,n}(\mu) = \sum_{i=1}^{N} (u_h^n(\mu), \Phi_i^h)\ \Phi_i^h$.

- The first term T_1 may be estimated using the inequality (19), such that

$$\left\| u(t)(\mu) - u_h^n(\mu) \right\|_{H^1(\Omega)} \leq C(\mu)\ (h + \Delta t_F). \tag{35}$$

- We denote by $\mathcal{S}_h = \{u_h(\mu, t), \mu \in \mathcal{G}, t \in [0, T]\}$ the set of all the solutions. For our model problem, this manifold has a low complexity. It means that for an accuracy $\varepsilon = \varepsilon(N)$ related to the Kolmogorov N-width of the manifold $\mathcal{S}_h$, for any $\mu \in \mathcal{G}$, and any $n \in 0, \dots, N_T$, T_2 is bounded by ε which depends on the Kolmogorov N-width.

$$T_2 = \left\| u_h^n(\mu) - \sum_{i=1}^{N} (u_h^n(\mu), \Phi_i^h)\ \Phi_i^h \right\|_{H^1(\Omega)} \leq \varepsilon(N). \tag{36}$$

- The third term T_3 depends on the method used to create the RB.

  1. Let us first consider the greedy approach with a Gram-Schmidt procedure and an eigenvalue problem (28), which yields to an orthogonalization in L^2 and in H_1. Therefore,

$$\left\| u_{hh}^{N,n} - u_{Hh}^{N,n} \right\|_{H^1(\Omega)}^2 = \sum_{i=1}^{N} |(u_h^n(\mu) - \widetilde{u_H}^n(\mu), \Phi_i^h)|^2 \left\| \Phi_i^h \right\|_{H^1(\Omega)}^2, \tag{37}$$

where $\widetilde{u_H}^n(\mu)$ is the quadratic interpolation of the coarse snapshots on time t^n $\forall n = 0, \dots, N_T$, defined by (25). Indeed, we want to recover the second order in time of the Crank-Nicolson scheme and a linear reconstruction in time leads to suboptimal bounds [20].
From the RB orthonormalization in L_2, the equation (28) yields

$$\left\|\Phi_i^h\right\|_{H^1}^2 := \left\|\nabla\Phi_i^h\right\|_{L^2(\Omega)}^2 = \lambda_i \left\|\Phi_i^h\right\|_{L^2(\Omega)}^2 = \lambda_i \leq \max_{i=1,\cdots,N} \lambda_i = \lambda_N, \tag{38}$$

such that the equation (37) yields

$$\left\|u_{hh}^{N,n} - u_{Hh}^{N,n}\right\|_{H^1(\Omega)}^2 \leq C\lambda_N \left\|u_h^n(\mu) - \widetilde{u_H}^n(\mu)\right\|_{L^2(\Omega)}^2. \tag{39}$$

Now by definition of $\widetilde{u_H}^n(\mu)$ and by theorem 26, for $t^n \in I_m$,

$$\left\|u_h^n(\mu) - \widetilde{u_H}^n(\mu)\right\|_{L^2} \leq \left\|u_h^n(\mu) - \widetilde{u_h}(t^n)(\mu)\right\|_{L^2} + \left\|u_h(t^n)(\mu) - \widetilde{u_H}^n(\mu)\right\|_{L^2} \leq C(\mu)(H^2 + \Delta t_F), \text{ since } \Delta t_G^2 \simeq \Delta t_F, \tag{40}$$

and we end up for equation (39) with

$$\left\|u_{hh}^{N,n} - u_{Hh}^{N,n}\right\|_{H^1(\Omega)} \leq C\sqrt{\lambda_N}(H^2 + \Delta t_G^2), \tag{41}$$

where C does not depend on N. Combining these estimates (35), (36) and (41), we obtain the estimate (31).

2. Now we consider only an L^2-orthonormalized basis, which we will denote $(\Psi_{h,i})_{i=1,\dots,N}$ (obtained by a Gram-Schmidt algorithm or with the Greedy-POD algorithm 1). The functions $(\Psi_{h,i})_{i=1,\dots,N}$ and $(\Phi_i^h)_{i=1,\dots,N}$ are both generators of X_h^N. Thus, there exists $(\gamma^i)_{i=1,\dots,N} \in \mathbb{R}^N$ such that $\Psi_{h,i} = \sum_{j=1}^{N} \gamma_j^i \Phi_i^h$.
By the H^1-orthogonality of the $(\Phi_i^h)_{j=1,\dots,N}$, it follows

$$\begin{aligned}
\left\|\Psi_{h,i}\right\|_{H^1}^2 &= \sum_{j=1}^{N} |\gamma_j^i|^2 \left\|\Phi_i^h\right\|_{H^1}^2, \\
&\leq \lambda_N \sum_{j=1}^{N} |\gamma_j^i|^2 \left\|\Phi_i^h\right\|_{L^2(\Omega)}^2 \text{ by equation (28)}, \\
&= \lambda_N \left\|\Psi_{h,i}\right\|_{L^2(\Omega)}^2 \text{ by the } L^2\text{-orthogonality of the } (\Psi_{h,i}^n)_{i=1,\dots,N}.
\end{aligned} \tag{42}$$

From the estimate (42) and the L_2-orthonormalization of the RB,

$$\begin{aligned}
\left\|u_{hh}^{N,n}(\mu) - u_{Hh}^{N,n}(\mu)\right\|_{H^1} &\leq \sum_{i=1}^{N} |(u_h^n(\mu) - \widetilde{u_H}^n(\mu), \Psi_{h,i}^n)| \left\|\Psi_{h,i}\right\|_{H^1}, \\
&\leq C\sqrt{\lambda_N} \sum_{i=1}^{N} |(u_h^n(\mu) - \widetilde{u_H}^n(\mu), \Psi_{h,i})|.
\end{aligned} \tag{43}$$

From Cauchy-Schwarz inequality, inequality (43) leads to

$$\begin{aligned}
\left\|u_{hh}^{N,n}(\mu) - u_{Hh}^{N,n}(\mu)\right\|_{H^1} &\leq C\sqrt{\lambda_N}\sqrt{N} \sqrt{\sum_{i=1}^{N} |(u_h^n(\mu) - \widetilde{u_H}^n(\mu), \Psi_{h,i})|^2}, \\
&\leq C\sqrt{\lambda_N}\sqrt{N} \left\|u_h^n(\mu) - \widetilde{u_H}^n(\mu)\right\|_{L^2(\Omega)},
\end{aligned}$$

and we end up with

$$\left\|u_{hh}^{N,n}(\mu) - u_{Hh}^{N,n}(\mu)\right\|_{H^1} \leq C\sqrt{N}\sqrt{\lambda_N}(H^2 + \Delta t_G^2), \tag{44}$$

which leads to estimate (31) using the inequalities (35), (36), and (44), and concludes the proof.

□

Remark 4.4. *Note that, from the proof of Theorem 4.1, the estimate of the method implemented with an only L^2 orthonormalized basis set has an additional $\sqrt{N}$ factor (where N is the number of modes) compared to the one obtained from the L^2 and H^1 orthogonalized basis set. Thus, the NIRB approximation is stabilized with the H^1 orthogonality, compared with a RB only orthogonalized in L^2. This difference may be numerically observed on more complex numerical results which require more modes [11].*

L^2 estimate. We proceed with the proof of theorem 4.3.

Proof. In analogy with the H^1 estimate, we have

$$\forall n = 0, \dots, N_T, \left\| u(t^n)(\mu) - u_{Hh}^{N,n}(\mu) \right\|_{L^2} \leq \left\| u(t^n)(\mu) - u_h^n(\mu) \right\|_{L^2} + \left\| u_h^n(\mu) - u_{hh}^{N,n}(\mu) \right\|_{L^2} + \left\| u_{hh}^{N,n}(\mu) - u_{Hh}^{N,n}(\mu) \right\|_{L^2}$$
$$=: T_1 + T_2 + T_3. \tag{45}$$

- For the first term T_1, it follows theorem 2.4 that

$$T_1 \leq C(h^2 + \Delta t_F). \tag{46}$$

- As with the H^1 estimate, T_2 can be estimated with the Kolmogorov N-width, and thus, for an accuracy $\varepsilon' = \varepsilon'(N) \leq \varepsilon(N)$,

$$T_2 \leq \varepsilon'. \tag{47}$$

- For the last term T_3, by L^2-orthonormality,

$$\left\| u_{hh}^{N,n}(\mu) - u_{Hh}^{N,n}(\mu) \right\|_{L^2(\Omega)}^2 = \sum_{i=1}^{N} |(u_h^n(\mu) - u_H^n(\mu), \Psi_{h,i}^n)|^2 \left\| \Phi_i^h S \right\|_{L^2(\Omega)}^2,$$
$$\leq C \left\| u_h^n(\mu) - u_H^n(\mu) \right\|_{L^2(\Omega)^2}. \tag{48}$$

  By theorem 26 and triangle inequality, it leads to

$$\left\| u_{hh}^{N,n}(\mu) - u_{Hh}^{N,n}(\mu) \right\|_{L^2(\Omega)}^2 \leq C\ (H^2 + \Delta t_G^2). \tag{49}$$

  Combining (45) with (46), (47), (49) concludes the proof.

□

5 Numerical results.

In this section, we applied the NIRB algorithm on several numerical tests and in each case, we compared NIRB errors without the rectification post-treatment with rectified NIRB errors 3:

- First, on the model problem (8) with $\Delta t_G \simeq H \simeq \frac{h}{2} \simeq \frac{\Delta t_F}{2}$. Note that in some situations, because of the constants C_2 and C_4 in the estimate of theorem 4.1, the best size for the coarse mesh may not be $\Delta t_F^{1/2}$. We observe that the NIRB with and without the rectification gives the same accuracy as with the fine solutions.
- Then, on the model problem with $\Delta t_G^2 \simeq H \simeq \sqrt{h} \simeq \Delta t_F$. The error with the NIRB method is reduced compared to the coarse FEM errors, and with the rectification post-treatment, we retrieve the fine FEM errors. We retrieved the rates of convergence expected from theorem 4.1 in $\mathcal{O}(h + \Delta t_F)$ for both with and without the rectification post-processing algorithm.
- Finally, we also tested our problem on a more complex problem, which is the Brusselator equations, and retrieved the fine accuracy with the NIRB and the rectification postprocessing algorithms.

We implemented both schemes on FreeFem ++ (version 4.9) [15] in order to retrieve the fine and coarse snapshots, and save the solutions in VTK format (with $u_0 = 0$). Then we applied the NIRB/ NIRB rectified algorithm with python, in order to highlight the non-intrusive side of this method (as in [11]). After saving the NIRB approximations with Paraview module on Python, the errors have been computed with FreeFem++.

5.1 $\Delta t_G \simeq H \simeq \frac{h}{2} \simeq \frac{\Delta t_F}{2}$.

We took $\mathcal{G} = (0, 10)$ and as our right-hand side function

$$f(t, \mathbf{x}) = 10[x^2(x-1)^2y^2(y-1)^2 - 2t((6x^2-6x+1)(y^2(y-1)^2) + (6y^2-6y+1)(x^2(x-1)^2))], \tag{50}$$

where $\mathbf{x} = (x, y)$.

We took 19 parameters in $\mathcal{G}$ for the RB construction such that $\mu_i = 0.5i,\ i = 1, \ldots, 19$ and $t_0 = 1$, and $T = 2$ (note that the coarse time grid must belong to the interval of the fine one). We tried our algorithms on several size of meshes, always with $\Delta t_F \simeq h$ and $\Delta t_G \simeq H$ (both schemes are stables).

Figure 1 presents the results of the NIRB algorithm (with POD-Greedy) for a new parameter $\mu = 1$ (so we removed this parameter for the construction of the snapshots). We plotted the H_0^1 errors both with and without the rectification post-treatment, and these errors are compared to the fine and coarse FEM errors. The exact solution is given by

$$u(t, \mathbf{x}; 1) = 10tx^2(1-x)^2y^2(1-y)^2.$$

The rectification post-processing step is done for each time step. Thus the NIRB with rectification is given by

$$R^n[u_{Hh}^N(\mu)] = \sum_{i,j=1}^{N} R_{ij}^n\ \alpha_j^H(\mu, t^n)\ \Phi_i^h(\mathbf{x}),\ n \geq 0, \tag{51}$$

where the rectification matrix R may be seen as an indexed (by n) familly of 2nd-order tensor.

The relative errors are computed in the maximum-norm in time. The H_0^1 NIRB error is defined as

$$\frac{\left\| u(\mu) - u_{Hh}^N(\mu) \right\|_{L^\infty(t_0,T;H_0^1(\Omega))}}{\left\| u(\mu) \right\|_{L^\infty(t_0,T;H_0^1(\Omega))}}, \tag{52}$$

and with the rectification post-treatment we have

$$\frac{\left\| u(\mu) - R[u_{Hh}^N(\mu)] \right\|_{l^\infty(t_0,\ldots,N_T;H_0^1(\Omega))}}{\left\| u(\mu) \right\|_{L^\infty(t_0,T;H_0^1(\Omega))}}, \tag{53}$$

where $R[u_{Hh}^N]$ is defined by (51), and these relative errors are compared to the FEM ones defined as

$$\frac{\left\| u(\mu) - u_h(\mu) \right\|_{L^\infty(t_0,T;H_0^1(\Omega))}}{\left\| u(\mu) \right\|_{L^\infty(t_0,T;H_0^1(\Omega))}} \text{ and } \frac{\left\| u(\mu) - u_H(\mu) \right\|_{L^\infty(t_0,T;H_0^1(\Omega))}}{\left\| u(\mu) \right\|_{L^\infty(t_0,T;H_0^1(\Omega))}}. \tag{54}$$

We also plotted the L^2 errors in Figure 2. We can see that the NIRB L^2 relative error without rectification is very close to the coarse L^2 relative error, thus, in the L^2 norm, no amelioration is provided by the NIRB algorithm, however with the rectification post-treatment, the error reaches the fine accuracy.

Finally, in order to evaluate the NIRB algorithm with respect to the parameters, table 1 presents the maximum H_0^1-error of the NIRB rectified approximation over the parameters. The error is given by

$$\max_{\mu \in \mathcal{G}_{Ntrain}} \frac{\left\| u_h(\mu) - [Ru_{Hh}^N(\mu)] \right\|_{l^\infty(t_0,\ldots N_T;H_0^1(\Omega))}}{\left\| u_h(\mu) \right\|_{L^\infty(t_0,T;H_0^1(\Omega))}}. \tag{55}$$

and the maximum in our training parameters is retrieved for $\mu = 9$.

5.1.1 Time execution (min,sec)

We present the FEM and NIRB runtimes in 2 and 3.

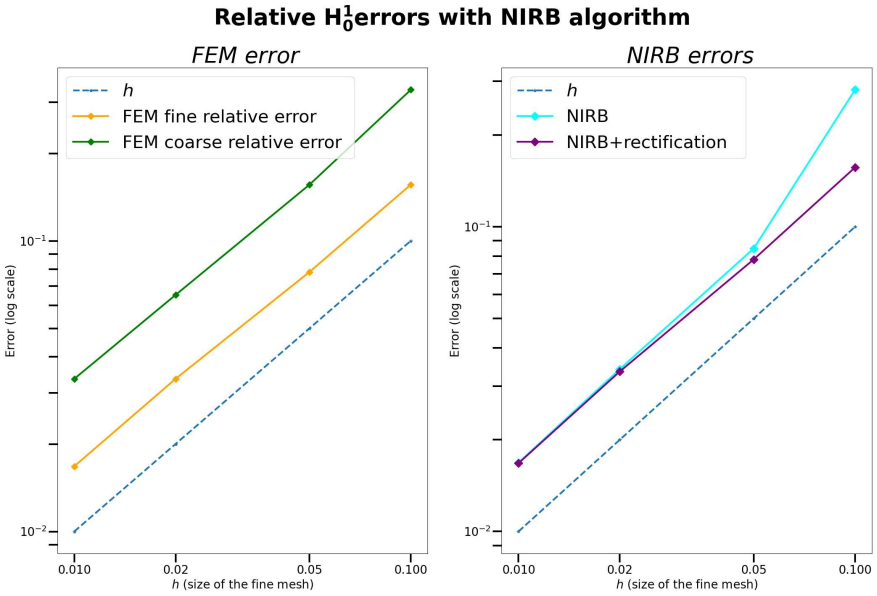

Figure 1: $\Delta t_G \simeq H \simeq \frac{h}{2} \simeq \frac{\Delta t_F}{2}$. Convergence rate for $\mu = 1$ (as a new parameter): FEM H_0^1 relative errors (54) for several sizes of mesh (left) compared to the NIRB method with ($N = 3$) and without the rectification post-treatment ($N = 3$) (right) (53)

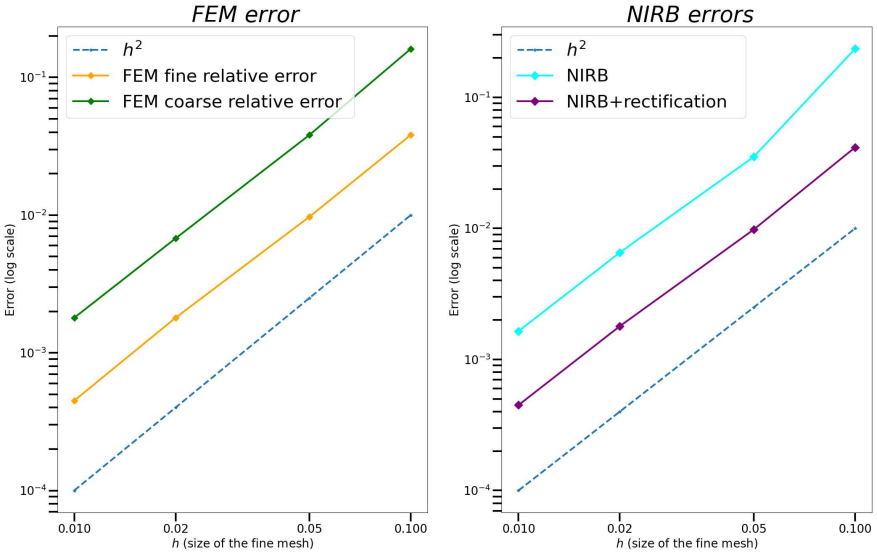

Figure 2: $\Delta t_G \simeq H \simeq \frac{h}{2} \simeq \frac{\Delta t_F}{2}$. Convergence rate for $\mu = 1$ (as a new parameter): FEM L^2 relative errors for several sizes of mesh (left) compared to NIRB with ($N = 3$) and without the rectification post-treatment ($N = 3$) (right)

Table 1: Maximum H_0^1 error over the parameters [$\mu = 9$] (55) (compared to the true NIRB projection and to the FEM coarse projection) with $N = 20$ with $h = 0.01$

NIRB rectified error	$\max_{\mu \in \mathcal{G}_{Ntrain}} \frac{\|u_h(\mu) - u_{hh}^N(\mu)\|_{L^\infty(t_0,T;H_0^1(\Omega))}}{\|u_h(\mu)\|_{L^\infty(t_0,T;H_0^1(\Omega))}}$	$\max_{\mu \in \mathcal{G}_{Ntrain}} \frac{\|u_h(\mu) - u_H(\mu)\|_{L^\infty(t_0,T;H_0^1(\Omega))}}{\|u_h(\mu)\|_{L^\infty(t_0,T;H_0^1(\Omega))}}$
4.84×10^{-5}	2.31×10^{-10}	1.42×10^{-1}

Table 2: FEM runtimes

FEM high fidelity solver	FEM coarse solution
00:03	00:02

Table 3: NIRB runtimes ($N = 10$)

NIRB Offline	classical rectified NIRB online
1:45	00:02

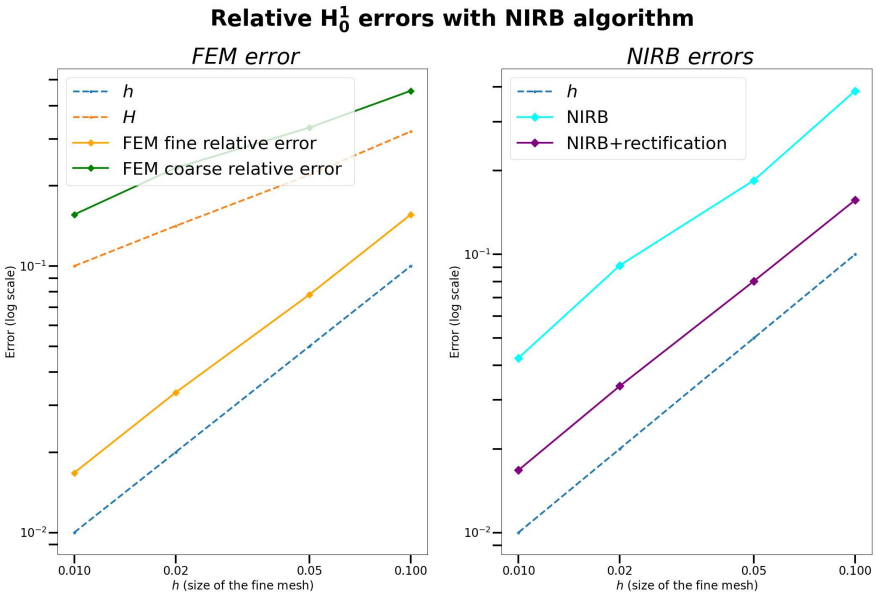

Figure 3: $H^2 \simeq h \simeq \Delta t_G^2 \simeq \Delta t_F$, Convergence rate for $\mu = 1$ (as a new parameter): FEM relative H_0^1 errors for several sizes of mesh (left) compared to NIRB with (N=3) and without the rectification post-treatment ($N = 3$) (right)

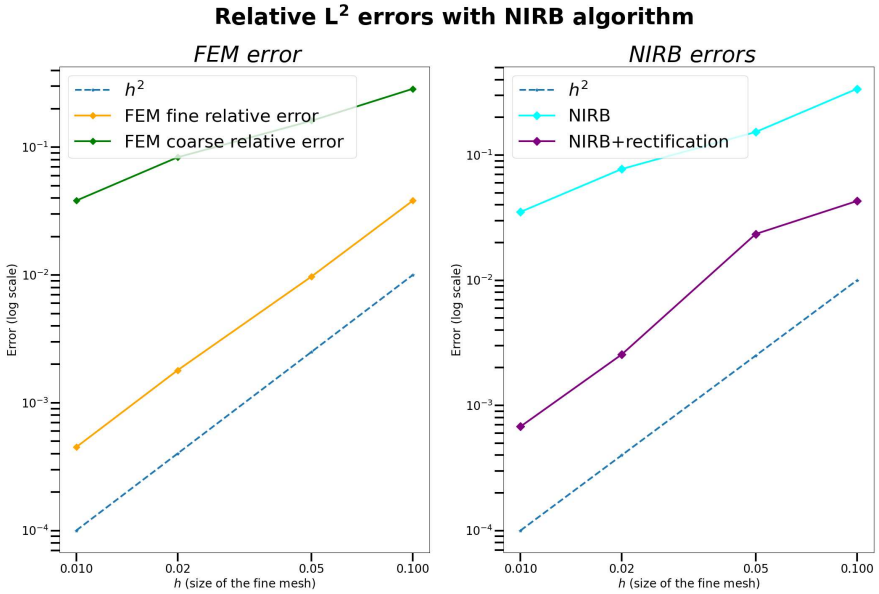

Figure 4: $H^2 \simeq h \simeq \Delta t_G^2 \simeq \Delta t_F$, Convergence rate for $\mu = 1$ (as a new parameter): FEM L^2 relative errors for several sizes of mesh (left) compared to NIRB with ($N = 3$) and without the rectification post-treatment ($N = 3$) (right)

5.2 $H^2 \simeq h \simeq \Delta t_G^2 \simeq \Delta t_F$

As previously, in Figure 3 we display the convergence rate of the fine approximations (left) and of the NIRB approximations (with and without rectification). For all meshes, we choose $\mu = 1$ and as expected, we observe that both NIRB errors converge in $\mathcal{O}(h + \Delta t_F)$, and we retrieved the fine accuracy with the rectified approximation.

We also plotted the L^2 errors in Figure 4.

Finally, in order to evaluate the NIRB algorithm with respect to the parameters, table 4 presents the maximum H_0^1-error of the NIRB rectified approximation over the parameters. The error is given by (55), and the maximum in our training parameters is retrieved for $\mu = 9$.

Table 4: Maximum H_0^1 error over the parameters [$\mu = 9$] (55) (compared to the true NIRB projection and to the FEM coarse projection) with $N = 20$ with $h = 0.01$

NIRB rectified error	$\max_{\mu \in \mathcal{G}_{Ntrain}} \frac{\|u_h(\mu) - u_{hh}^N(\mu)\|_{L^\infty(t_0,T;H_0^1(\Omega))}}{\|u_h(\mu)\|_{L^\infty(t_0,T;H_0^1(\Omega))}}$	$\max_{\mu \in \mathcal{G}_{Ntrain}} \frac{\|u_h(\mu) - u_H(\mu)\|_{L^\infty(t_0,T;H_0^1(\Omega))}}{\|u_h(\mu)\|_{L^\infty(t_0,T;H_0^1(\Omega))}}$
4.21×10^{-3}	1.40×10^{-9}	7.80×10^{-1}

5.2.1 Time execution (min,sec)

We present the FEM and NIRB runtimes in 5 and 6.

Table 5: FEM runtimes

FEM high fidelity solver	FEM coarse solution
00:03	00:01

We observe that the errors without the rectification post-treatment increases with N due to the role of the constants C_2 and C_4 in the estimate of theorem 4.1, whereas with the post-treatment they remain stable. This is illustrated by Figure 5 where the H_0^1 errors are displayed for $\mu = 1$ and different number of modes N.

Table 6: NIRB runtimes ($N = 10$)

NIRB Offline	classical rectified NIRB online
1:32	00:02

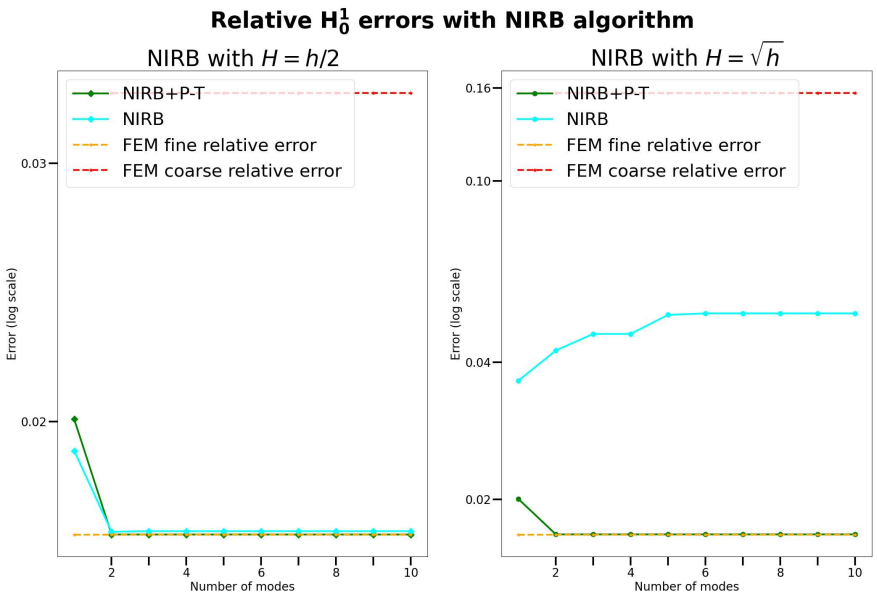

Figure 5: For $h = 0.01$: $H = \frac{h}{2}$ (left) , $H = h^2$ (right) $\mu = 1$, NIRB relative H_0^1 errors and rectified NIRB (+ P-T) H_0^1 compared to FEM errors with different modes N

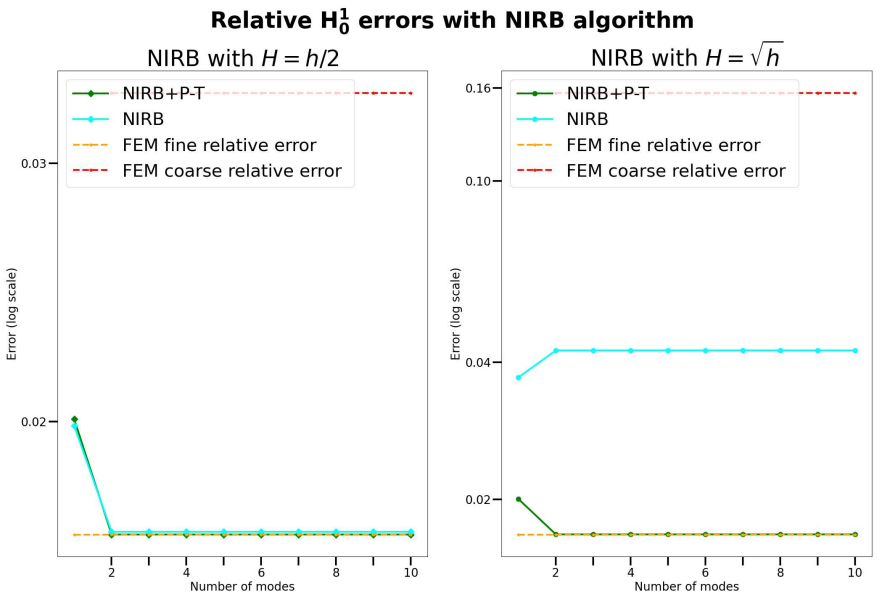

Figure 6: For $h = 0.01$: $H = 2h$ (left) , $H = h^2$ (right) $\mu = 1$, NIRB relative H_0^1 errors and rectified NIRB (+ P-T) H_0^1 compared to FEM errors with different modes N using the other NIRB decomposition (56)

Remark 5.1. *We may also consider NIRB aproximations of* (14) *under the form*

$$u_{Hh}^{N,n}(\boldsymbol{x};\mu) = \sum_{i=1}^{N} \alpha_i^H(\mu, t^n)\ \Phi_{h,i}^n(\boldsymbol{x}),\ n \geq 0, \tag{56}$$

with $(\Phi_{h,i}^n)_{i=1,..,N}$ *time-dependent basis functions. This time, the greedy algorithm 2 is executed for each time step and thus, this method is less efficient (in term of storage) since we have to store* N *times the number of time steps of the reduced basis.*

With this decomposition, we obtained the following results (see Figure 6).

5.3 Brusselator equations

We consider a last test more complex, involving chemical reactions, which is the Brusselator problem [21]. For this problem, the chemical concentrations are controlled by parameters throughout the reaction process, which makes it interesting as an application of our NIRB method. Indeed, this problem may be seen as an optimization problem over the parameters. Thus, let us consider the Brusselator problem in a spatial domain $\Omega = [0,1]^2$ and with an ending time $T = 5$. The two-dimensional reaction–diffusion Brusselator system is the non-linear system of partial differential equations (with Neumann boundary conditions)

$$\begin{cases} \partial_t u_1 = a + u_1 u_2^2 - (b+1)u_1 + \alpha \Delta u_1, \text{ in } \Omega \times]0,T] \\ \partial_t u_2 = b u_1 - u_1\, u_2^2 + \alpha \Delta u_2, \text{ in } \Omega \times]0,T], \\ u_1(\mathbf{x},0) = u_0(\mathbf{x}) = 2 + 0.25y, \text{ in } \Omega \\ u_2(\mathbf{x},0) = v_0(\mathbf{x}) = 1 + 0.8x, \text{ in } \Omega, \\ \partial_n u_1 = 0, \ \partial\Omega, \\ \partial_n u_2 = 0, \ \partial\Omega. \end{cases}$$

Now, we have to deal with a non-linearity, and two unknowns. Our parameter belongs to $\mathbb{R}^3$, $\boldsymbol{\mu} = (a, b, \alpha)$. For the implementations, we use an Euler implicit scheme for the fine solutions with the Newton algorithm to deal with the non-linearity and an explicit 2nd order Runge-Kutta scheme (RK2) for the coarse mesh (thus the coarse approximation is computed much faster). Indeed, with an explicit Euler scheme, the solution blows up whereas for a scheme of order 2 (as RK2) it is stable for our parameters.

We tested our NIRB algorithm on stable solutions ($b \leq 1 + a^2$). For α small enough, the solutions (u_1, u_2) converge to $(u_l, v_l) = (a, \frac{b}{a})$, which may be verified by our NIRB approximation bellow as presented in Figure 8,

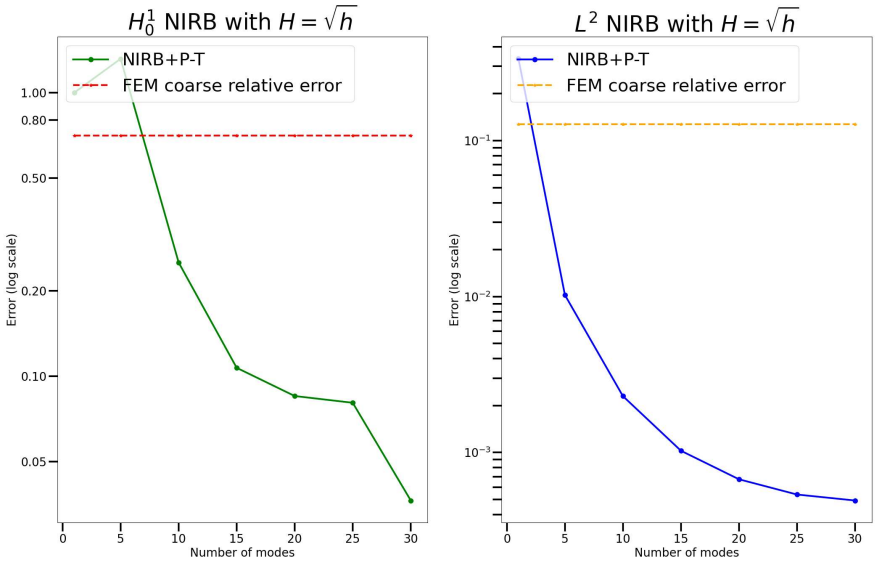

Figure 7: Test with $L^\infty(0,T;H^1(\Omega))$ relative errors with a new parameter $(a,b,\alpha) = (3,2,0.008)$, $t_0 = 0$, $T = 5$, $\Omega = [0,1] \times [0,1]$ (NIRB+ rectification post-treatment compared to coarse FEM error)

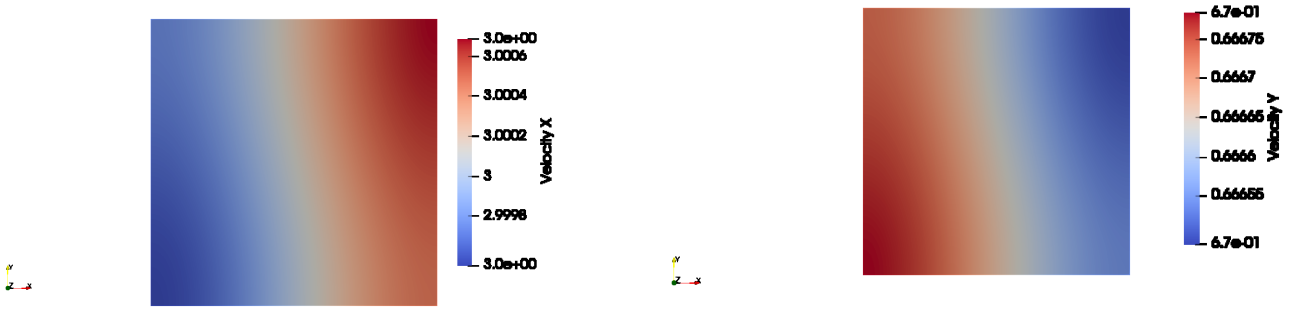

(a) u_1 (b) u_2

Figure 8: NIRB approximations (u_1 (left) and u_2 (right)) for $T = 5$ with $N = 10$ modes (close to $(a, \frac{b}{a}) = (3, 2/3)$)

thus we choose several snapshots with the parameters $(a,b,\alpha) \in [2,4] \times [1,4] \times [0.001, 0.05]$, and more precisely we took $a = 2, 2.5, 4$, $b = 1, 3, 4$ and $\alpha = 0.001,\ 0.005,\ 0.01,\ 0.05$, and tested our algorithm on the new parameter $(a,b,\alpha) = (3,2,0.008)$ with $h = 0.02 = \Delta t_F \simeq H^2 = \Delta t_G^2$ ($\Delta T_G = H = 0.1$). The relative H_0^1 errors of the NIRB approximation with rectification post-treatment (53) and of the FEM fine approximation (54)) are displayed in Figure 7. Here, we do not know the exact solution but we observe a gain of accuracy of factor 10 with 25 modes on the relative H_0^1 error with the NIRB solution compared to the coarse FEM one (with 30 modes, the error drops to 3.64×10^{-2}, compared to 7.06×10^{-1} with the FEM approximation).

In Figure 8 follows the NIRB rectified solution for $N = 10$ modes at time $T = 5$ for the two variables u_1 and u_2. The approximation is close to $(a, \frac{b}{a}) = (3, 2/3)$ as expected.

Finally, the computational costs are well saved during the online part of the algorithm as it is highlited with this example. Indeed, since there is a non-linearity, the system must be solved several times for each time step, and thus is quite expensive for a high-fidelity approximation.

5.3.1 Time execution (min,sec)

We present the FEM and NIRB runtimes in 7 and 8.

Table 7: FEM runtimes (min:sec)

FEM high fidelity solver	FEM coarse solution
4:52	00:02

Table 8: NIRB runtimes ($N = 10$, h:min:sec)

NIRB Offline	classical rectified NIRB online
1:53:00	00:04:00

6 Estimates on the rectification

As observed in our numerical results, the rectification post-treatment allows us to retrieve the error of the fine solutions. This section aims to understand how it works and takes its inspiration from a previous work [19]. We refer to chapter 7 of [19] for the notations.

In the elliptic context, the rectification matrix is defined by (3), whereas in the parabolic context, it is given by algorithm 3, where a loop in time takes place. Thus, for each time step, the rectification post-treatment works as in the elliptic framework, hence we will stick to the unique notation without the time indices.

In both cases, we deal with three linear operators:

- $\pi_N : V_h \to X_h^N$, which represents our fine solutions.
- $\mathcal{I}_N : V_H \subset V_h \to X_h^N$, which is our coarse solutions.
- $\tilde{\pi}_N : V_H \subset V_h \to X_h^N$, which is our rectification operator, which goes from coarse to fine coefficients.

Notation:
u_{hh}^N: true approximation, u_{Hh}^N: NIRB approximation, Ru_{Hh}^N : Rectified NIRB approximation.

By definition,

$$Ru_{Hh}^N(\mu_k) = u_{hh}^N(\mu_k), \forall k = 1, \dots, N. \tag{57}$$

For $k = 1, \dots, N$,

$$\begin{aligned}
\left\| \sum_{i=1}^{N} (u_h(\mu), \Phi_i^h)\Phi_i^h - \sum_{i,j=1}^{N} R_{i,j}(u_H(\mu), \Phi_j^h)\Phi_i^h \right\|_{H^1(\Omega)} &\leq \left\| \sum_{i=1}^{N} (u_h(\mu) - u_h(\mu_k), \Phi_i^h)\Phi_i^h - \sum_{i,j=1}^{N} R_{i,j}(u_H(\mu) - u_H(\mu_k), \Phi_j^h)\Phi_i^h \right\|_{H^1(\Omega)}, \\
&\leq \sqrt{\lambda_N} \left\| u_h(\mu) - u_h(\mu_k) \right\|_{L^2(\Omega)} + \left\| \sum_{i,j=1}^{N} R_{i,j}(u_H(\mu) - u_H(\mu_k), \Phi_j)\Phi_i \right\|_{H^1(\Omega)}, \\
&\leq \sqrt{\lambda_N} [\left\| u_h(\mu) - u_h(\mu_k) \right\|_{L^2(\Omega)} + \|\tilde{\pi}_N\|_2 \left\| u_H(\mu) - u_H(\mu_k) \right\|_{L^2}].
\end{aligned}$$

Since the Kolmogorov width is small,

$$E(\mathcal{M}_h, X_h^N) = \sup_{x \in \mathcal{M}_h} \left(\inf_{y \in X_n^h} \left\| x - y \right\| \right) \tag{58}$$

is small and thus,

$$\inf \left\| u_h(\mu) - \Phi_h(\mu_k) \right\| \leq E(\mathcal{M}_h, X_h^N) \tag{59}$$

is small too. Now, $\left\| u_H(\mu) - u_H(\mu_k) \right\|_{L^2}$ must be small, so the Kolmogorov width of the coarse solutions needs to be relatively small too. We may numerically prove in our problem model that $\|\tilde{\pi}_N\|_2$ is in $\mathcal{O}(1)$.

References

[1] M. Barrault, C. Nguyen, A. Patera, and Y. Maday. An 'empirical interpolation' method: application to efficient reduced-basis discretization of partial differential equations. *Comptes rendus de l'Académie des sciences. Série I, Mathématique*, 339-9:667–672, 2004.

[2] G. Berkooz, P. Holmes, and J L Lumley. The proper orthogonal decomposition in the analysis of turbulent flows. *Annual review of fluid mechanics*, 25(1):539–575, 1993.

[3] S. Brenner and R. Scott. *The mathematical theory of finite element methods*, volume 15. Springer Science & Business Media, 2007.

[4] A. Buffa, Y. Maday, A. T. Patera, C. Prud'homme, and G. Turinici. A priori convergence of the greedy algorithm for the parametrized reduced basis method. *ESAIM: Mathematical Modelling and Numerical Analysis-Modélisation Mathématique et Analyse Numérique*, 46(3):595 – 603, 2012.

[5] F. Casenave, A. Ern, and T. Lelièvre. A nonintrusive reduced basis method applied to aeroacoustic simulations. *Advances in Computational Mathematics*, 41(5):961–986, Jun 2014.

[6] R. Chakir. *Contribution à l'analyse numérique de quelques problèmes en chimie quantique et mécanique*. PhD thesis, 2009. Doctoral dissertation, Université Pierre et Marie Curie-Paris VI.

[7] R. Chakir and Y. Maday. A two-grid finite-element/reduced basis scheme for the approximation of the solution of parametric dependent p.d.e. In *9e Colloque national en calcul des structures*, 2009.

[8] R. Chakir, Y. Maday, and P. Parnaudeau. A non-intrusive reduced basis approach for parametrized heat transfer problems. *Journal of Computational Physics*, 376:pp.617–633, January 2019.

[9] R. Chakir, B. Streichenberger, and P. Chatellier. A non-intrusive reduced basis method for urban flows simulation. 01 2021.

[10] L. C. Evans. *Partial differential equations*. American Mathematical Society, Providence, R.I., 2010.

[11] E. Grosjean. *Variations and further developments on the Non-Intrusive Reduced Basis two-grid method*. PhD thesis, 2022. Thèse de doctorat dirigée par Maday, Yvon Mathématiques appliquées Sorbonne université 2022.

[12] E. Grosjean and Y. Maday. Error estimate of the non-intrusive reduced basis method with finite volume schemes. *ESAIM: M2AN*, 55(5):1941–1961, 2021.

[13] B. Haasdonk. Convergence rates of the pod–greedy method. *ESAIM: Mathematical modelling and numerical Analysis*, 47(3):859–873, 2013.

[14] B. Haasdonk and M. Ohlberger. Reduced basis method for finite volume approximations of parametrized linear evolution equations. *ESAIM: Mathematical Modelling and Numerical Analysis-Modélisation Mathématique et Analyse Numérique*, 42(2):277–302, 2008.

[15] F. Hecht. New development in freefem++. *Journal of numerical mathematics*, 20(3-4):251–266, 2012.

[16] J. S. Hesthaven, G. Rozza, and B. Stamm. *Certified reduced basis methods for parametrized partial differential equations*. Springer, 2016.

[17] D J. Knezevic and A T. Patera. A certified reduced basis method for the fokker–planck equation of dilute polymeric fluids: Fene dumbbells in extensional flow. *SIAM Journal on Scientific Computing*, 32(2):793–817, 2010.

[18] A. Kolmogoroff. Über die beste annaherung von funktionen einer gegebenen funktionenklasse. *Annals of Mathematics*, pages 107–110, 1936.

[19] Y. Maday and O. Mula. A generalized empirical interpolation method: application of reduced basis techniques to data assimilation. In *Analysis and numerics of partial differential equations*, pages 221–235. Springer, 2013.

[20] C. Makridakis. Space and time reconstructions in a posteriori analysis of evolution problems. In *ESAIM: Proceedings*, volume 21, pages 31–44. EDP Sciences, 2007.

[21] R.C. Mittal and R. Jiwari. Numerical solution of two-dimensional reaction–diffusion brusselator system. *Applied Mathematics and Computation*, 217(12):5404–5415, 2011.

[22] A. Quarteroni, A. Manzoni, and F. Negri. *Reduced Basis Methods for Partial Differential Equations: an introduction*, volume 92. Springer, 2015.

[23] B. Streichenberger. *Approches multi-fidélités pour la simulation rapide d'écoulements d'air en milieu urbain*. PhD thesis, 2021. Thèse de doctorat, Université Gustave Eiffel.

[24] V. Thomée. *Galerkin finite element methods for parabolic problems*, volume 25. Springer Science & Business Media, 2007.